Korean J. Chem. Eng., 38(3), 505-513 (2021)
DOI: 10.1007/s11814-020-0706-z

pISSN: 0256-1115
eISSN: 1975-7220

Adsorption performance and mechanism investigation of Mn^{2+} by facile synthesized ceramsites from lime mud and coal fly ash

Changjin Ou, Suwan Dai, Shuxuan Li, Jie Xu, and Juan Qin†

Nantong Key Laboratory of Intelligent and New Energy Materials, School of Chemistry and Chemical Engineering, Nantong University, Nantong 222100, China

(*Received 29 June 2020 • Revised 28 October 2020 • Accepted 3 November 2020*)

Abstract−To efficiently control manganese pollution, two kinds of ceramsites with pH self-adjustment ability, being synthesized from lime mud and coal fly ash, were employed to remove Mn^{2+} from aqueous solutions. The influence of different parameters like contact time, concentration of Mn^{2+} and pH on adsorption performance was examined. Also, the mechanism of Mn^{2+} removal by the ceramsites was investigated thoroughly. The results showed that the maximum Mn^{2+} adsorption capacity of ceramsites was 2.54±0.03 mg/g and the time required to reach equilibrium was about 4h. The pseudo-second-order kinetic model and the Langmuir model could better describe the adsorption kinetic experimental data and isotherms process, respectively. During the adsorption process of Mn^{2+}, pH self-adjustment ability of ceramsites played a leading role in creating an alkaline environment to form precipitation $MnO(OH)_2$, which was subsequently adsorbed onto the surface of the ceramsites. This study suggests ceramsites with pH self-adjustment ability have enormous potential in the application for removing Mn^{2+} from wastewater.

Keywords: Adsorption, Mn^{2+} Removal, Ceramsites, pH self-adjustment, Lime Mud

INTRODUCTION

As a heavy metal, manganese (Mn) is widely distributed in nature. It has been estimated that the total storage of Mn in the world is about 500 million tons [1]. Specifically, Africa makes up the most proportion (180 million), following by the Ukraine (140 million), and China (44 million). Considering their strong oxidizing property, high permeability and resistivity, Mn compounds have a wide range of applications [2,3]. For example, 90% of the produced Mn is used for iron and steel industry, and the rest id applied to the nonferrous metallurgical industry, chemistry engineering, electronics, batteries, and agriculture [4-7].

Mn is an essential nutrient for metabolism, because it is a cofactor of many enzymes, such as transferases, hydrolases, lyases and so on. Thus, the moderate intake of Mn can promote the growth of bones and improve hematopoietic function of the body [8-10]. In contrast, chronic intake of more than 0.1 mg/L Mn can affect the function of the central and peripheral nervous systems, leading to irreversible neurological disorders [11]. And occupational exposure to Mn for more than six months can probably cause manganism, which exhibits symptoms similar to idiopathic Parkinson's disease [12,13]. Of course, Mn pollution also has effects on other organisms. For instance, acid wastewater drainage of Dabaoshan mine in Guangdong of China, mainly containing Pb, Cd, Mn and other heavy metals, has made the rivers downstream toxic, destroying the ecosystem of aquatic organisms and reducing the biodiversity [14]. Moreover, an abandoned manganese mine in Kgwakgwe, southeastern of Botswana, caused a high concentration of Mn in soils and then affected the concentration of Mn in vegetation, thereby causing local sparse vegetation [15]. Currently, while the global industry is boosting economic development, it is urgent to govern the production, use and disposal of Mn [16-20].

Mn pollution mainly results from industrial emissions and divalent manganese (Mn^{2+}) is the common form in industrial wastewater [21]. It has been reported that the concentration of Mn^{2+} in the inlets of sewage treatment plants in Hunan of China was between 28.38-2876 mg/L, while in the outlets was between 0.19-195 mg/L [22]. According to the Integrated Wastewater Discharge Standard (GB 8978-1996) of China, the maximum permissible emission concentration of total Mn is 5 mg/L, so there is an urgent requirement of a suitable method to remove Mn^{2+} from wastewater further [23]. Currently, the technologies used to remove Mn^{2+} include filtration, membrane process, ion-exchange, chemical precipitation, adsorption [24-28]. Among them, adsorption has attracted increasing attention due to its advantages of simplicity, economics reversibility, efficiency, and eco-friendliness [29]. As is known, the key to adsorption is adsorbents, so it is very desirable to develop a low-cost and efficient adsorbent for Mn^{2+}.

The paper industry is one of the main economic activities in many countries. In 2019, about 72 million tons of pulp was produced in China [30]. And the need for paper is still on the increase. Lime mud is a kind of by-product from alkali recycling in the paper industry [31]. It is estimated that about 0.5 tons of lime mud can be produced by one ton of pulp [32]. And it can be divided into two categories: from wood-based pulp and from non-wood pulp. It has been reported that the former can be reused in alkali recycling, while the latter is difficult to recycle due to the silica problem [33]. Therefore, a number of non-wood paper mills are con-

†To whom correspondence should be addressed.
E-mail: qinjuan880816@ntu.edu.cn

fronted with serious survival problems. In previous studies [34,35], a novel kind of ceramsite was discovered, which was prepared by high temperature solid state reaction method and using lime mud from non-wood pulp and coal fly ash as raw materials. The ceramsites have been proved to obtain stable physical and chemical properties, especially the pH self-adjustment ability, which are favorable for the precipitation and adsorption of heavy metals. In recent years, various ceramsites have been widely investigated and used as adsorbents to remove heavy metals, such as Pb, Cu, Cr, and Hg, from aqueous solutions [36-38]. Wang et al. [37] realized the adsorption of Cd^{2+} with ceramsites which were developed using different urban sediments. Jing et al. [38] used diatomite and tungsten residue to prepare ceramsites with the aim of removing Cu^{2+} from wastewater. However, the adsorption of Mn^{2+} with ceramsites was rarely studied, so the control of adsorption parameters and its mechanism are still unclear. Based on this, the functionalized ceramsites prepared in the previous studies [34,35] may be a promising adsorbent for Mn^{2+}.

The main objective of this study was to evaluate the feasibility of removing Mn^{2+} from aqueous solutions using two kinds of ceramsites with pH self-adjustment ability as adsorbents. Static adsorption experiments were carried out to illustrate the adsorption performance. The crucial factors, such as adsorbent kinds, contact time, concentration of Mn^{2+} and pH were, explored. The adsorption kinetics and equilibrium were further studied using the data obtained from these experiments. Finally, the adsorption mechanism of Mn^{2+} using ceramsites with pH self-adjustment ability was investigated deeply.

MATERIALS AND METHODS

1. Preparation of Adsorbents

The ceramsites were prepared from lime mud and coal fly ash. Lime mud was obtained from Xinda Paper Industry Co. Ltd (Jiangsu, China). Coal fly ash was obtained from Huaneng Nanjing Power Station (Jiangsu, China), which is a pulverized coal combustion power plant. The chemical composition of raw materials and preparation process of ceramsites can be referred to the previous study [34]. Particularly, the nomenclature and composition of ceramsites used in this study are shown in Table S1 (Supplementary Materials), and the final calcination temperature was 1,050 °C.

2. Characterization of Absorbents

Appropriate amount of sample was used for crystalline phase analysis by X-ray diffraction (XRD, Model D8 Advance, BRUKER, Germany). Morphological feature of the ceramsites was detailed using scanning electron microscope (SEM, Model Gemini SEM 300, ZEISS, Germany). Water absorption and bulk density were determined by the Archimedes method according to ASTM C373 [39]. Compressive strength was tested by an electronic universal tester (Model CMT5105, SANS Testing Machine Co., Ltd., China) according to BS EN 13055 [40]. Apparent porosity was measured according to ISO 18754 [41].

Ceramsites L50 and L60 were mixed uniformly, and then the leaching test was carried out according to BS EN 12457-2 [42]. The content of heavy metals was tested by inductively coupled plasma mass spectroscopy (ICP-MS, Model ICP-MS 2000, Jiangsu Skyray Instrument Co., Ltd., China). The test was conducted according to the analysis method of each determinand and the internal standard method was used for the quantitative analysis [43]. The concentration of Ca^{2+} in aqueous samples was determined by EDTA titration [44].

3. Batch Experiments

All chemical reagents used were of analytical grade. All solutions were prepared with deionized water. Mn^{2+} stock solution (1,000 mg/L, calculated by Mn element) was prepared by dissolving 3.6010 g of $MnCl_2{\cdot}4H_2O$ (Purity 99.99%) in 1 L of deionized water [45]. Solutions containing Mn^{2+} were prepared by diluting the stock solution to the desired concentration. NaOH (0.1 M) and HNO_3 (0.1 M) were used to adjust the pH of solution [17,46]. The concentration of Mn^{2+} in aqueous samples was measured by an ultraviolet spectrophotometer (Model UV-5200, Shanghai Yuanxi Instrument Co., Ltd., China) [47].

3-1. Static Leaching Experiments

To investigate the capacity of OH^- released by the ceramsites, 4 g of ceramsite L50 or L60 and 200 mL of deionized water were added to a conical flask [35]. Then the flasks were immersed in a water bath (Model HZQ-F100, Taicang Huamei Biochemical Instrument Factory, China) at 25 °C and shaken at 120 r/min. Aqueous samples were taken at predetermined intervals (0.5, 1, 2, 3, 6, 8, 10, 12, 16, 20, 24, 28, 40, 52, 64, 88, 136, 192 h) and then pH values were tested by a pH detector (Model FE28, METTLER TOLEDO, Switzerland).

3-2. Mn^{2+} Batch Adsorption Experiments

To evaluate the removal efficiency of Mn^{2+}, 4 g of ceramsite L50 or L60 and 200 mL of solution containing 5 mg/L Mn^{2+} were placed in each flask [48]. The flasks were immersed in a water bath at 25 °C and then shaken at 120 r/min. Aqueous samples were taken at predetermined intervals (0.5, 1, 1.5, 2, 3, 4, 6, 8, 10, 12, 16 h).

To investigate the effect of initial concentration of Mn^{2+} on adsorption, aqueous solutions with different concentrations of Mn^{2+} (5, 10, 15, 20, 25, 40, 60, 80 mg/L) were prepared [48]. The shaking time was 10 h and other operating conditions were as above.

To explore the effect of initial pH on adsorption, aqueous solutions with different initial pH values (2.83, 4.11, 6.74, 8.23) were prepared [48]. Ceramsites L50 and L60 were placed in solutions containing 15 and 20 mg/L Mn^{2+}, respectively. Other operating conditions were as above. All the experiments were conducted in triplicate.

4. Data Evaluation

4-1. Removal Efficiency of Mn^{2+} and Adsorption Capacity of the Ceramsites

The removal efficiency (R, %) and adsorption capacity (q_t, mg/g) of Mn^{2+} were calculated by Eqs. (1) and (2) [17,49]:

$$R=(C_0-C_t)/C_0\times100\% \quad (1)$$

$$q_t=(C_0-C_t)\times V/m \quad (2)$$

where C_0 (mg/L) was the initial concentration of Mn^{2+}; C_t (mg/L) was the concentration of Mn^{2+} at time t; V (L) was the solution volume; m (g) was the mass of adsorbent used.

4-2. Adsorption Kinetics of Mn^{2+}

To explore the adsorption process of Mn^{2+}, the pseudo-first-order

and pseudo-second-order models were applied to test the fitness of experimental data. The linear forms of the two models are shown in Eqs. (3) and (4), respectively [38,50]:

$$\ln(q_e-q_t)=\ln q_e-k_1t \quad (3)$$

$$t/q_t=1/k_2q_e^2+t/q_e \quad (4)$$

where t (h) is the adsorption time; q_e (mg/g) is the adsorption capacity at equilibrium; k_1 (1/h) is the rate constant of the pseudo-first-order model; k_2 [g/(mg·h)] is the rate constant of the pseudo-second-order model.

4-3. Adsorption Isotherms of Mn^{2+}

Langmuir and Freundlich models were used for equilibrium description. The former, as a theoretical model, assumes monolayer adsorption over an energetically homogeneous adsorbent surface. The latter, as an empirical model, is based on heterogeneous adsorption over independent sites. The two models could be represented by Eqs. (5) and (6) [38]:

$$C_e/q_e=1/q_mB+C_e/q_m \quad (5)$$

$$\lg q_e=\lg K_f+n\lg C_e \quad (6)$$

where C_e (mg/L) is the concentration of Mn^{2+} at equilibrium; B (L/mg) is the constant of Langmuir model; K_f [(mg/g)/(mg/L)$^{1/n}$] is the constant related to adsorption capacity of Freundlich model; n is the empirical constant related to adsorption properties of Freundlich model.

RESULTS AND DISCUSSION

1. Characterization of Ceramsites

XRD patterns and SEM images of ceramsites L50 and L60 before adsorption are shown in Fig. S1 (Supplementary Materials). Due to different content of lime mud used in preparing, anorthite ($CaAl_2Si_2O_8$) and gehlenite ($Ca_2Al_2SiO_7$) were found to be the main crystalline phases of ceramsites L50 and L60, respectively, as shown in Fig. S1(a) and (b). The previous study [35] proved that the more gehlenite is, the more OH^- is released, which is probably more favorable for the adsorption of Mn^{2+}. Moreover, the surfaces with many connected pores were observed in Fig. S1(c) and (d). Simultaneously, the high water absorption (>30%) and apparent porosity (>48%) were detected and presented in Table S2 (Supplementary Materials), indicating that the ceramsites were porous materials [51]. It has been reported that porous structures have large specific surface and specific surface energy, which may strengthen their adsorption capacity [51,52]. In addition, the mechanical strength of the two ceramsites was over 8 MPa, which was enough for practical application [53].

Since the ceramsites were a comprehensive utilization of solid wastes, it was necessary to detect their toxicity for future engineering applications. Toxicity leaching tests were conducted and the results are shown in Table 1. Compared with the identification standards for extraction toxicity between United States and China, it

Table 1. The results of leaching test

Item	Leaching concentration (mg/L)		Limited values (mg/L)	
	Lime mud	Ceramsites	United states[a]	China[b]
As^{3+}	0.0213	0.0110	5	5
Hg^{2+}	ND[c]	ND	0.2	0.1
Ag^{+}	ND	ND	5	5
Se	0.0927	0.0020	1	1
Cr^{3+}	2.1500	0.0965	5	15
Cd^{2+}	7.3300	0.4575	1	1
Cu^{2+}	0.0057	0.0145	NS[d]	100
Pb^{2+}	3.4000	0.5325	5	5
Zn^{2+}	0.1082	0.1605	NS	100
Ni^{2+}	0.1582	1.4995	NS	5
Be^{2+}	0.2000	0.0150	NS	0.02
Ba^{2+}	0.0175	0.0330	100	100

[a]Taken from U.S. Government Publishing Office. 40 CFR 261.24 - Toxicity characteristics

[b]Taken from GB 5085.3-2007

[c]ND=Not detected

[d]NS=Not specified

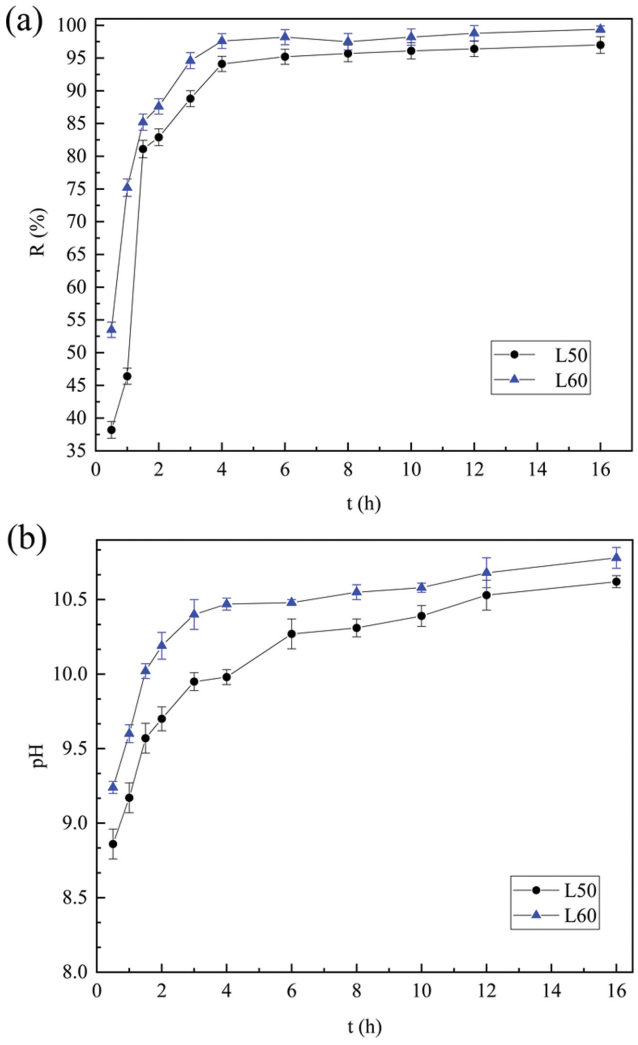

Fig. 1. Removal efficiency of Mn^{2+} and pH of solutions with different ceramsites at different contact time: (a) removal efficiency; (b) pH value.

can be seen that the limited values are stricter in China [54,55]. As for lime mud, the leaching concentrations of Cd^{2+} and Be^{2+} were 7.33 and 0.20 mg/L, respectively, which exceeded the limited values of 1 and 0.02 mg/L in China. As for the ceramsites, the concentration of toxic elements was much lower than the standards. Hu et al. [56] pointed out that heavy metals could be immobilized by forming new mineral phases during thermal treatment. Cheng et al. and Yang et al. [57,58] also proved the formation of aluminosilicates could enhance the immobilization of heavy metals. Therefore, it is likely that heavy metals in lime mud were immobilized during calcination. And the ceramsites could be classified as green materials.

2. Batch Adsorption Study

2-1. Effect of Contact Time

Fig. 1 presents the effect of contact time on Mn^{2+} adsorption. By increasing contact time, an increase in removal efficiency of Mn^{2+} was observed in Fig. 1(a). In most cases, the quick initial efficiency of adsorption occurred during the first few hours of contact, followed by a slower one until equilibrium state was reached. This was probably due to the existence of abundant active sites on the surfaces of the ceramsites, whereas as adsorption continued, a progressive saturation of these active sites with time occurred [17]. In addition, the required time to reach equilibrium was about 4 h, since an increase of contact time to 16 h did not have any significant effect. And the maximum removal efficiency of Mn^{2+} by ceramsites L50 and L60 was 97.0±1.3% and 99.4±0.5%, respectively.

Considering the pH self-adjustment ability of the ceramsites, pH changes during adsorption were monitored, as shown in Fig. 1(b). It was obvious that the pH increased quickly in 4 h from an initial value of 6.97±0.06, and then the rates of increase slowed significantly after the adsorption equilibrium was reached. Eventually the solutions were formed into an alkaline environment (about pH=10.5). OH^- consumed during adsorption could be replenished quickly and maintained at a relatively stable level finally, indicating that the pH self-adjustment ability of ceramsites was remarkable.

2-2. Effect of Initial Concentration of Mn^{2+}

The efficiency of metal adsorption from aqueous solutions is particularly dependent on the initial metal concentration [17]. According to the results shown in Fig. 2, a decrease in the removal efficiency of Mn^{2+} could be noticed as the initial concentration of Mn^{2+} was increased. The maximum Mn^{2+} adsorption capacity of ceramsites L50 and L60 was 2.31±0.03 and 2.54±0.03 mg/g,, respectively, when the initial concentration of Mn^{2+} was increased to 120 mg/L. This was due to the increase in the driving force for mass transfer, which was the concentration gradient. In addition, pH values before adsorption at different initial concentrations of Mn^{2+} were in the range of 5.9-7.0, while after adsorption they were detected and presented in Fig. 2. It is obvious that even at a high concentration of 120 mg/L, alkaline environment in solutions could still be maintained by the pH self-adjustment ability of ceramsites. And ceramsite L60 performed slightly better than L50 in Mn^{2+} removal.

2-3. Effect of Initial pH

In the adsorption process of heavy metals, the pH of aqueous solutions is one of the most important controlling parameters, since it affects the surface charge of the adsorbents, the degree of ioniza-

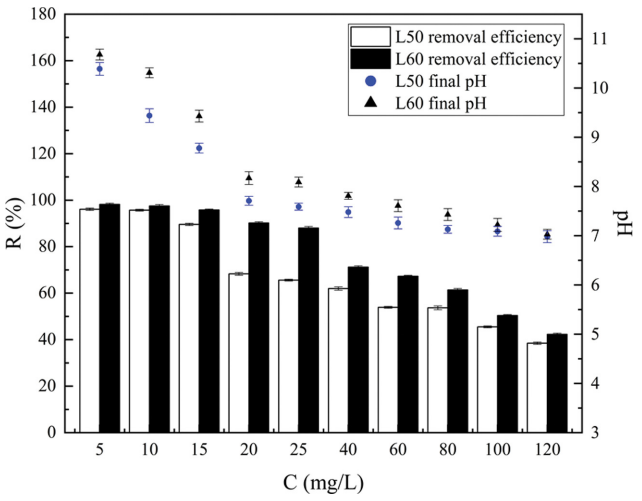

Fig. 2. Removal efficiency of Mn^{2+} and pH of solutions at different initial concentration of Mn^{2+}.

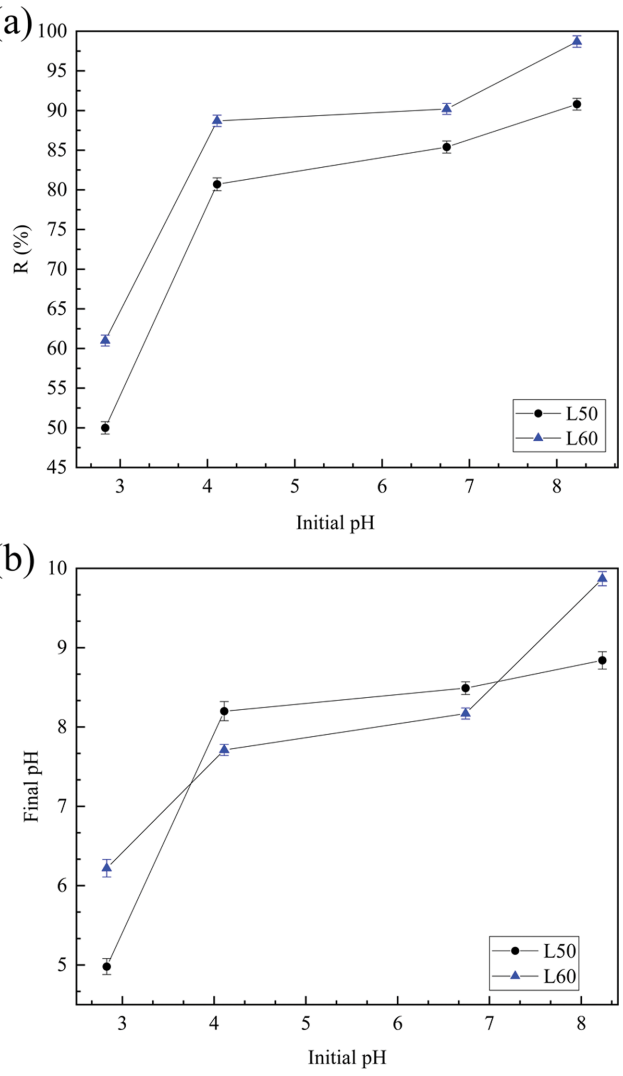

Fig. 3. Removal efficiency of Mn^{2+} and pH of solutions at different initial pH: (a) removal efficiency; (b) pH value.

tion and speciation of the heavy metals [59]. This study was carried out in a pH range of 3-8 since the precipitation of Mn^{2+} starts to form above pH 8 and wastewater containing Mn^{2+} is generally in a pH range of 4-7 [60]. As shown in Fig. 3(a), the removal efficiency of Mn^{2+} increased with the increasing pH value. At pH 2.83, the removal efficiency of Mn^{2+} by ceramsites L50 and 60 was 50.0±0.78% and 61.0±0.68%, respectively. For pH>4, the removal efficiency of Mn^{2+} was increased significantly and kept above 80%. The optimum removal efficiency of Mn^{2+} by ceramsites L50 and L60 was 90.8±0.74% and 98.7±0.73%, respectively, observed at pH 8.23. In fact, at lower pH values the solutions contained high concentration of H^+, which would compete with Mn^{2+} for OH^- released from the ceramsites and the active sites on the ceramsites. When the pH value was increased, the concentration of H^+ was decreased, resulting in greater adsorption of Mn^{2+}. It could be also concluded that ceramsite L60 performed better than L50 in Mn^{2+} removal. According to Fig. 3(b), it is obvious that the final pH value also increased with the increasing initial pH value. Even in an acidic solution, the ceramsites could still adjust the pH to alkalinity by producing OH^- spontaneously. Therefore, the initial pH range of wastewater containing Mn^{2+} could be greatly extended when the ceramsites are applied as adsorbents. Moreover, it was unnecessary to dose pH adjustment reagents, which significantly simplified the operation and saved the cost.

3. Adsorption Kinetics and Isotherms of Mn^{2+}

3-1. Adsorption Kinetics Models of Mn^{2+}

The pseudo-first-order and pseudo-second-order kinetic models were plotted for ceramsites L50 and L60 in Fig. 4. The results indicated that the adsorption of Mn^{2+} in this study was better described by the pseudo-second-order kinetic model. This was demonstrated by the correlation coefficient values (R^2=0.99 and 0.99), which were higher than those obtained from the pseudo-first-order kinetic model (R^2=0.86 and 0.77). What's more, the values of $q_{e,cal}$ (0.25 and 0.25 mg/g) calculated from the pseudo-second-order model were very close to the experimental data (0.24±

Table 2. The Langmuir and Freundlich parameters for Mn^{2+} adsorption by ceramsites L50 and L60

Sample No.	The Langmuir model			The Freundlich model		
	q_m	B	R^2	K_f	n	R^2
L50	2.57	9.89	0.93	0.49	2.81	0.92
L60	2.65	9.89	0.98	0.70	2.99	0.96

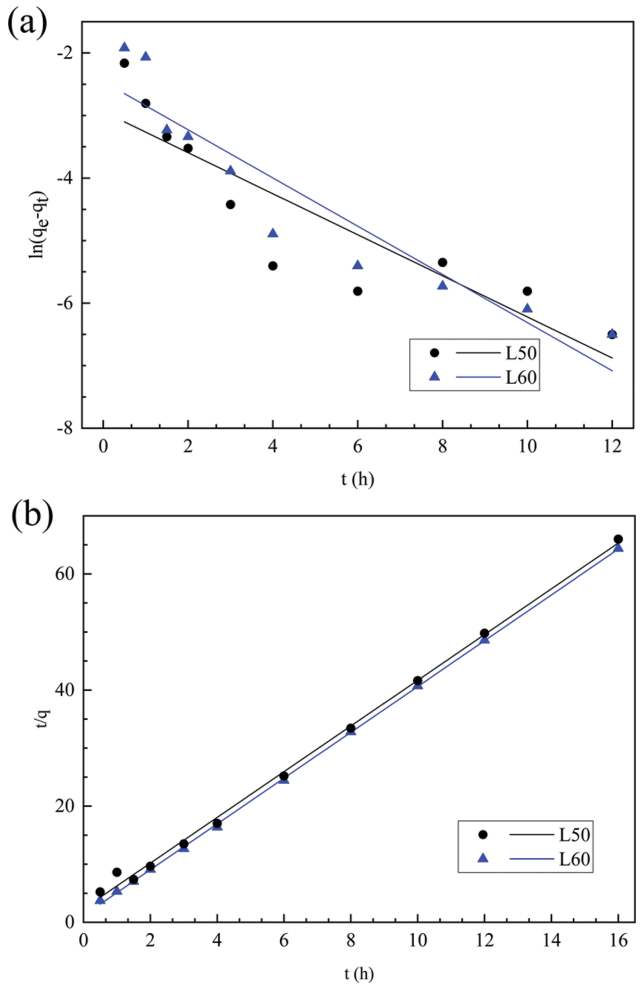

Fig. 4. Linear fitting plots of adsorption kinetics models: (a) the pseudo-first-order model; (b) the pseudo-second-order model.

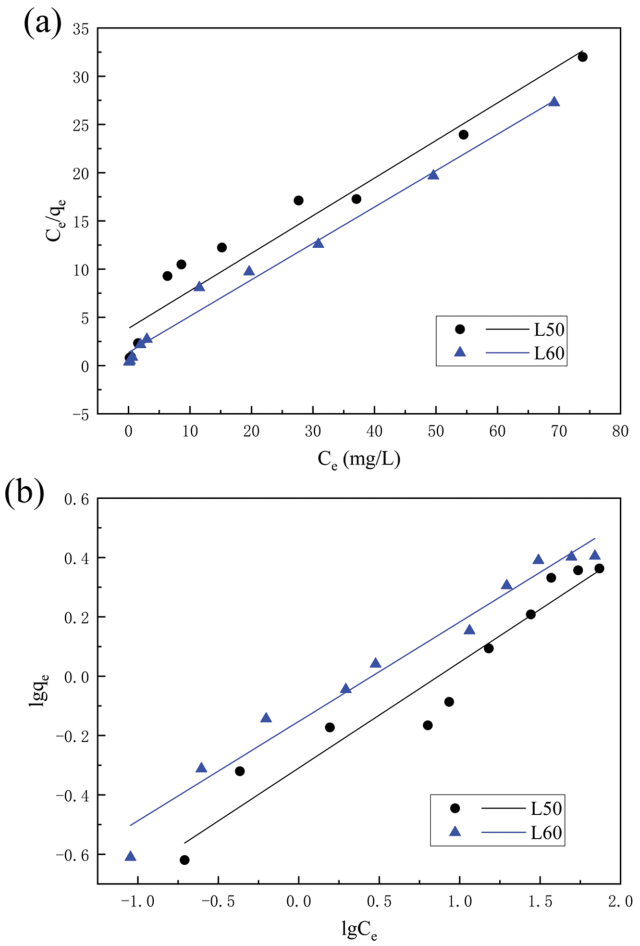

Fig. 5. Linear fitting plots of adsorption isotherm models: (a) the Langmuir model; (b) the Freundlich model.

0.003 and 0.25±0.001 mg/g). Therefore, it could be concluded that the adsorption of Mn^{2+} by the ceramsites was kinetically controlled by external film diffusion, surface adsorption and intraparticle diffusion [38].

3-2. Adsorption Isotherms Models of Mn^{2+}

The results obtained from the Langmuir and Freundlich isotherms models for ceramsites L50 and L60 are shown in Table 2 and Fig. 5. The data was fitted more smoothly into Langmuir isotherm model with high correlation coefficient (R^2=0.93 and 0.98) compared to the Freundlich isotherm model (R^2=0.92 and 0.96). The q_m values of ceramsites L50 and L60 calculated from the Langmuir model were 2.57 and 2.65 mg/g, respectively, which were relatively consistent with the experimental results (q_e=2.31±0.03 and 2.54±0.03 mg/g). Thus, it could be demonstrated that the adsorption of Mn^{2+} using the ceramsites was a process of monolayer chemical adsorption. Moreover, the comparison of the maximum adsorption capacities indicated that ceramsite L60 has more superior adsorption capacity for Mn^{2+} than L50.

4. Mechanism of Mn^{2+} Removal

Fig. 6 compares XRD patterns of ceramsites L50 and L60 before and after adsorption. The main crystalline phases of ceramsites L50 and L60 after adsorption were still anorthite and gehlenite, respectively. This meant that there were no significant changes in the composition of crystalline phases and the intensity of their diffraction peaks, indicating favorable chemical stability of the ceramsites. However, diffuse peaks appeared in the range of 2θ=10-15°, which demonstrated that a small amount of amorphous phase was formed. These changes could be attributed to the hydration reactions of anorthite and gehlenite with lattice imperfection, as shown in chemical formulas (7) and (8). Therefore, it is likely that the solution formed alkaline environment spontaneously where Mn^{2+} and OH^- were combined to form $Mn(OH)_2$ precipitation. Then, $Mn(OH)_2$ precipitation would be adsorbed onto the surface of ceramsites. Since ceramsite L60 with gehlenite as the main crystalline phase could release more OH^- [33], it showed better Mn^{2+} removal ability than L50.

$$CaAl_2Si_2O_8+3H_2O=Ca^{2+}+2OH^-+Al_2[Si_2O_5][OH]_4 \quad (7)$$

$$2Ca_2Al_2SiO_7+9H_2O=4Ca^{2+}+6OH^-+2Al[OH]_4^-+Al_2[Si_2O_5][OH]_4 \quad (8)$$

To better exhibit the pH self-adjustment ability, the efficiency of OH^- released by different ceramsites in the deionized water was examined and the results are shown in Fig. 7. It can be observed that there was a rapid increase of pH value in the first few hours (about 0-6 h), and then an equilibrium with pH values around 11 was reached. In addition, the ability of releasing OH^- by the ceramsites was efficient and enduring. By comparing Figs. 1(b) and 7, it can be noticed that the pH after Mn^{2+} adsorption was slightly lower. Absolutely, OH^- ions were consumed during adsorption, which might be combined with Mn^{2+} to form $Mn(OH)_2$ precipitation. However, the consumed OH^- would be compensated persistently by OH^- released from the ceramsites until adsorption equilibrium was reached.

Fig. 8 compares the microstructure and element composition of ceramsite L60 before and after adsorption. Before adsorption, ceramsite L60 was mainly composed of columnar, cubic and plate-

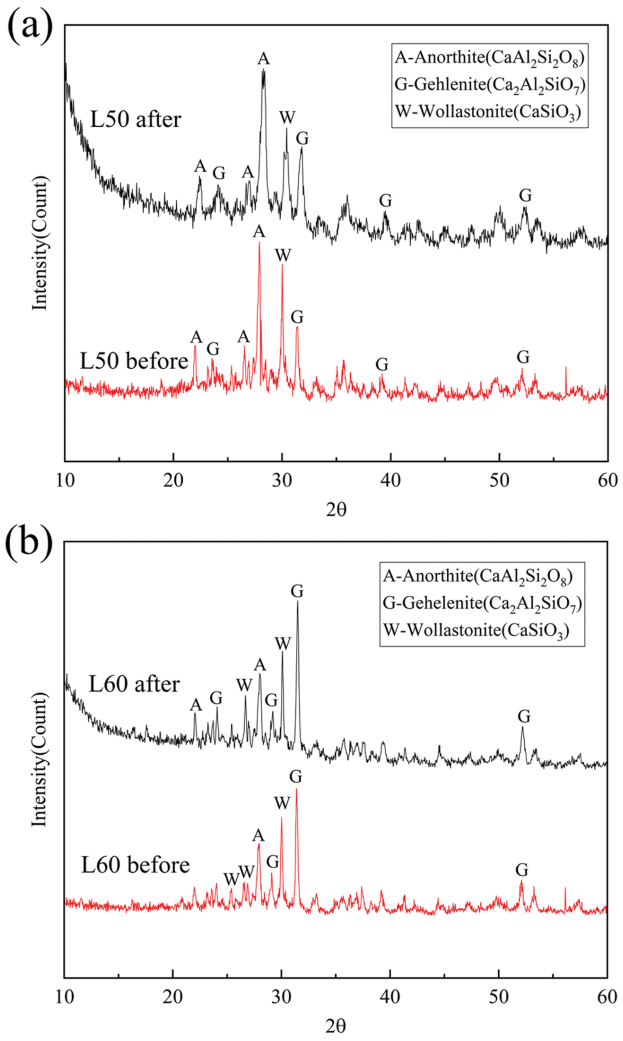

Fig. 6. The XRD patterns of the ceramsites: (a) before adsorption; (b) after adsorption.

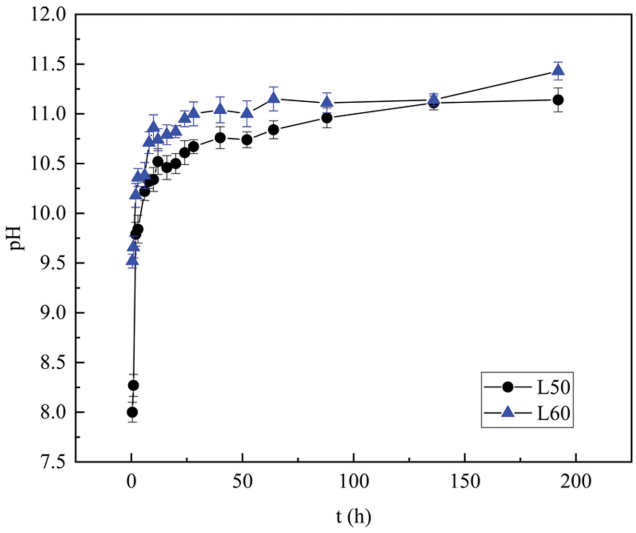

Fig. 7. pH values of the deionized water in contact with different ceramsites.

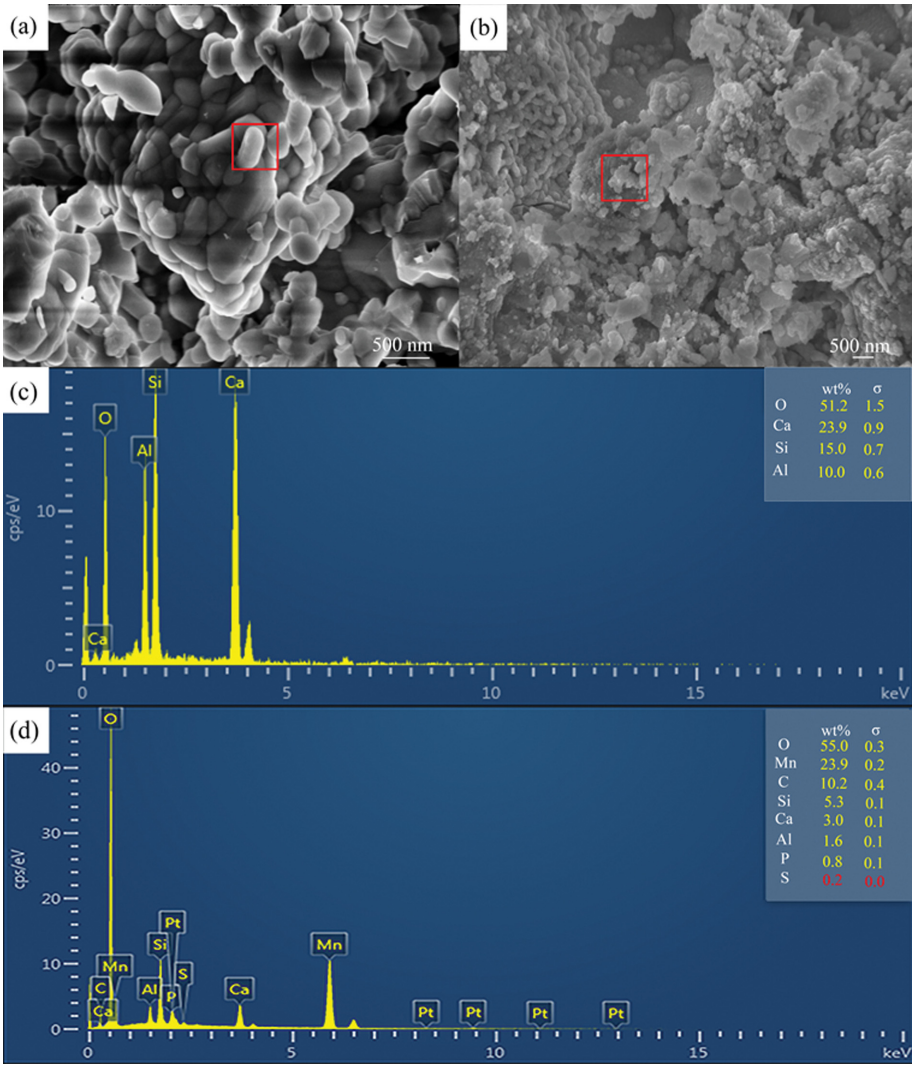

Fig. 8. SEM images and EDS analyses of ceramsite L60: (a) SEM before adsorption; (b) SEM after adsorption; (c) EDS before adsorption; (d) EDS after adsorption.

like grains and the surface was relatively rough. As shown in Fig. 8(b), after adsorption a layer of floccule was formed on the surface and the roughness was dropped. Furthermore, comparing Fig. 8(c) and (d), the peak of Mn was found after adsorption. It could be inferred that the floccule as the precipitation of Mn^{2+} was successfully adsorbed onto the surface of ceramsite L60. The photographs of ceramsite L60 before and after adsorption are shown in Fig. 9. It is conspicuous that the surface of ceramsite L60 was covered with a layer of brown compound after adsorption. As we know, $Mn(OH)_2$ is white and easily oxidized. Even if there is just a little oxygen in solutions, it would be transformed into brown $MnO(OH)_2$, as shown in chemical formula (9) [61]. Therefore, it could be concluded that Mn^{2+} in solutions reacted with OH^- released from the ceramsites to form $Mn(OH)_2$ and quickly oxidized to brown $MnO(OH)_2$ to be adsorbed on the surface of the ceramsites.

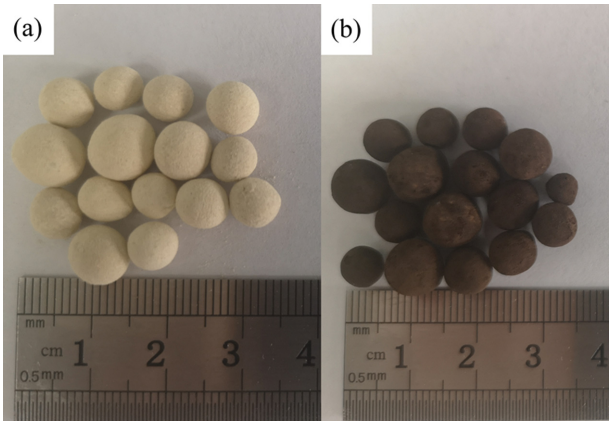

Fig. 9. Photographs of ceramsite L60: (a) before adsorption; (b) after adsorption.

$$2Mn(OH)_2+O_2=2MnO(OH)_2 \quad (9)$$

According to chemical formulas (7) and (8), it could not be ignored that Ca^{2+} was released simultaneously. To investigate the mechanism of Mn^{2+} removal further, the molar amount of Ca^{2+}

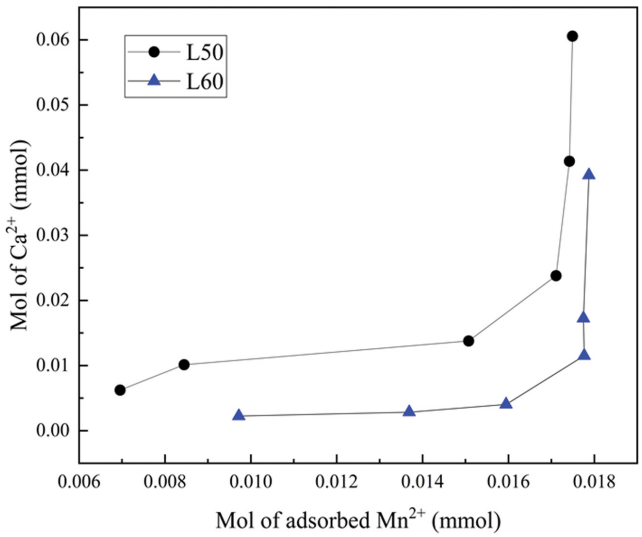

Fig. 10. Molar of released Ca^{2+} vs molar of adsorbed Mn^{2+} with ceramsites as adsorbents.

released and Mn^{2+} adsorbed at contact time of 0.5, 1, 2, 4, 8 and 10 h was measured, and then their relationship was fitted in Fig. 10. It can be seen that more Mn^{2+} was adsorbed on ceramsite L60 than L50 at the same point in time, which indicated the better adsorption performance of ceramsite L60. Since the amount of Ca^{2+} released did not have a linear relationship with the amount of Mn^{2+} adsorbed, it could be inferred that the mechanism of adsorption between ceramsites and solutions containing Mn^{2+} was not dominated by the ion-exchange model. What's more, the increasing trend of Ca^{2+} was strengthened after contacting of 2 h. As demonstrated above, the Langmuir monolayer adsorption model could describe the adsorption process in this study well. Therefore, the surface of the ceramsites was probably covered with $MnO(OH)_2$ in the first two hours, blocking the release of Ca^{2+} from ceramsites. However, due to the consumption of OH^- and capillary effect, Ca^{2+} was released in quantity eventually. In most engineering applications, the treated water containing Ca^{2+} and Al^{3+} is usually reused to treat wastewater containing phosphorus [62]. Therefore, it could be concluded that the ceramsites have low risk of causing secondary contamination and are environmentally friendly.

CONCLUSION

Ceramsites with pH self-adjustment ability prepared from lime mud and coal fly ash were removed Mn^{2+} from aqueous solutions successfully. The adsorption parameters and mechanism were investigated clearly. Time required to reach adsorption equilibrium was about 4 h. When the initial concentration of Mn^{2+} was between 5-20 mg/L, the removal efficiency was above 90%. The ceramsites could create alkaline environment by releasing OH^- spontaneously to ensure the formation of precipitation $MnO(OH)_2$, which was subsequently adsorbed onto the surface of the ceramsites. Considering the excellent adsorption performance of the ceramsites, future investigations of different contaminants (Cd^{2+}, Pb^{2+}, Hg^{2+}, PO_4^{3-} etc.) and actual water samples should be performed.

ACKNOWLEDGEMENTS

This work was financially supported by the National Natural Science Foundation of China (No. 51802162 and 51708302), Natural Science Foundation of Jiangsu Province (No.BK20180955) and Nature Science Foundation of Jiangsu Higher Education Institution of China (No.17KJB610008).

DISCLOSURE STATEMENT

The authors declare that they have no conflict of interest.

SUPPORTING INFORMATION

Additional information as noted in the text. This information is available via the Internet at http://www.springer.com/chemistry/journal/11814.

REFERENCES

1. J. Beukes, E. P. W. Nicolas, Swindell and H. Wabo, *Episodes*, **39**, 285 (2016).
2. M. Z. Ahsan, M. A. Islam and F. A. Khan, *Results Phys.*, **19**, 103402 (2020).
3. M. D. Drahus, P. Jackes and E. Erdem, *Phys. Rev. B*, **84**, 064113 (2011).
4. G. Hils, A. Newirkowez and M. Kroker, *Steel Res. Int.*, **86**, 411 (2015).
5. Y. Shao, *Resour. Conserv. Recycl.*, **117**, 25 (2017).
6. B. Saravanakumar, X. S. Wang, W. G. Zhang, L. D. Xing and W. S. Li, *Chem. Eng. J.*, **373**, 547 (2019).
7. W. P. Weiss and M. T. Socha, *J. Anim. Sci.*, **82**, 118 (2004).
8. J. W. Spears, *Biol. Trace Elem. Res.*, **188**, 35 (2019).
9. D. C. Oliveira, A. Nogueira-Pedro and E. W. Santos, *Nutr. Res. Rev.*, **31**, 267 (2019).
10. M. Kim, E. Kim and M. Choi, *Trace Elem. Electrolytes*, **30**, 51 (2013).
11. J. Shu, H. Wu, M. Chen, H. Peng, B. Li, R. Liu, Z. Liu, B. Wang, T. Huang and Z. Hu, *Water Res.*, **153**, 229 (2019).
12. M. Cersosimo and W. Koller, *Neurotoxicology*, **27**, 340 (2006).
13. Y. Y. Wang, J. Xue, S. Q. Cheng, Y. B. Ding, J. L. He, X. Q. Liu, X. M. Chen, Y. X. Wang, X. Y. Feng and Y. Y. Xia, *Int. J. Occup. Med. Environ. Health*, **25**, 501 (2012).
14. Y. Wang, R. Dong and Y. Z. Zhou, *Sci. Total Environ.*, **679**, 346 (2019).
15. G. I. E. Ekosse, P. S. Fouche and B. Mashatola, *Int. J. Environ. Sci. Technol.*, **3**, 15 (2006).
16. N. Marsidi, H. Abu Hasan and S. R. S Abdullah, *J. Water Process Eng.*, **23**, 1 (2018).
17. F. M. Pellera, A. Giannis, D. Kalderis, K. Anastasiadou, R. Stegmann, J. Y. Wang and E. Gidarakos, *J. Enviorn. Manage.*, **96**, 35 (2012).
18. M. Sasmaz, E. Öbek and A. Sasmaz, *Appl. Geochem.*, **100**, 287 (2019).
19. S. Fabiana, G. Marianela, N. Cintia, M. Cecilia and S. Karim, *J. Environ. Chem. Eng.*, **3**, 253 (2015).
20. S. Yang, D. Zhang and H. Cheng, *Anal. Chim. Acta*, **1074**, 54 (2019).

21. C. C. Kan, M. C. Aganon and C. M. Futalan, *J. Environ. Sci.-China*, **25**, 1483 (2013).
22. Q. M. Zhang, C. Ma, R. J. Xiang, Z. Liu and C. Chen, *Nonferr. Met. Sci. Eng.* (In Chinese), **5**, 95 (2014).
23. GB 8979-1996, Integrated Wastewater Discharge Standard, (In Chinese) (1996).
24. X. Tian, R. F. Zhang and T. L. Huang, *J. Environ. Sci.-China*, **77**, 346 (2019).
25. L. C. Ferreira, L. C. Ferreira, V. L. Cardoso and U. Coutinho, *J. Water Process Eng.*, **29**, 100792 (2019).
26. Y. C. Zhang, S. Z. Ni and X. J. Wang, *Chem. Eng. J.*, **372**, 82 (2019).
27. C. C. Kan, M. C. Aganon, C. M. Futalan and M. L. P. Dalida, *J. Environ. Sci.-China*, **25**, 1483 (2013).
28. J. P. Vistuba, M. E. Nagel-Hassemer and F. R. Lapolli, *Environ. Technol.*, **34**, 275 (2013).
29. M. A. Islam, D. W. Morton, B. B. Johnson and B. Mainali, *J. Water Process Eng.*, **26**, 264 (2018).
30. http://www.chinappi.org/reps/20190508092527140869.html, (In Chinese) (Accessed October 27th 2020).
31. J. Cheng, J. H. Zhou and J. Z. Liu, *Energy Fuels*, **23**, 2506 (2009).
32. F. M. Martins, J. M. Martins, L. C. Ferracin and C. J. da Cunha, *J. Hazard. Mater.*, **147**, 610 (2007).
33. J. Qin, C. Cui, C. M. Yang, X. Y. Cui, B. Hu and J. T. Huang, *J. Clean Prod.*, **113**, 355 (2016).
34. J. Qin, C. Cui, X. Y. Cui, H. Ahmad and C. M. Yang, *Constr. Build. Mater.*, **95**, 10 (2015).
35. J. Qin, C. M. Yang, C. Cui, J. T. Huang, H. Ahmad and H. L. Ma, *J. Environ. Sci.-China*, **47**, 91 (2016).
36. J. X. Dong, Y. H. Wang, L. J. Wang, S. J. Wang, S. J. Li and Y. Ding, *J. Water Process Eng.*, **34**, 101 (2020).
37. J. L. Wang, Y. L. Zhao, P. P. Zhang, L. Q. Yang, H. A. Xu and G. P. Xi, *Chin. J. Chem. Eng.*, **26**, 96 (2018).
38. Q. X. Jing, Y. Y. Wang, L. Y. Chai, C. J. Tang, X. D. Huang, H. Guo, W. Wang and W. You, *Trans. Nonferrous Met. Soc. China*, **28**, 1053 (2018).
39. ASTM C-20, Standard Test Methods for Apparent Porosity, Water Absorption, Apparent Specific Gravity, and Bulk Density of Burned Refractory Brick and Shapes by Boiling Water (2010).
40. BS EN 13055, Lightweight Aggregates (2016).
41. ISO 18754, Fine Ceramics (Advanced Ceramics, Advanced Technical Ceramics) - Determination of Density and Apparent Porosity (2020).
42. BS EN 12457-2, Characterisation of Waste - Compliance Test for Leaching of Granular Waste Materials and Sludges - Part 2 (2002).
43. S. H. Liang, J. T. Chen, M. X. Guo, D. L. Feng, L. Liu and T. Qi, *Waste Manage.*, **105**, 425 (2020).
44. J. Kim and C. Vipulanandan, *Cem. Concr. Res.*, **33**, 621 (2003).
45. H. Choi, N. C. Woo, M. Jiang, F. S. Cannon and S. A. Snyder, *Sep. Purif. Technol.*, **136**, 184 (2014).
46. X. Y. Zhang, J. Zhou, Y. B. Fan and J. Y. Liu, *Korean J. Chem. Eng.*, **37**, 1445 (2020).
47. Y. Cheng, W. Y. Xiong and T. L. Huang, *Sci. Total Environ.*, **737**, 139525 (2020).
48. S. Bandar, M. Anbia and S. Salehi, *J. Alloys Compd.*, **851**, 156822 (2021).
49. L. Y. Duan, X. D. Hu, D. S. Sun, Y. Z. Liu, Q. J. Guo, T. K. Zhang and B. T. Zhang, *Korean J. Chem. Eng.*, **37**, 1166 (2020).
50. Z. Sareban and V. Javanbakht, *Korean J. Chem. Eng.*, **34**, 2886 (2017).
51. S. Suresh, K. Kante, E. H. Fini and T. J. Bandosz, *Micropor. Mesopor. Mater.*, **286**, 155 (2019).
52. Y. J. Shao, B. Ren, H. M. Jiang, B. J. Zhou, L. P. LV, J. Z. Ren, L. C. Dong, J. Li and Z. F. Liu, *J. Hazard. Mater.*, **333**, 222 (2017).
53. J. L. Zou, G. R. Xu and G. B. Li, *J. Hazard. Mater.*, **165**, 995 (2019).
54. 40 CFR 261.24 - Toxicity Characteristics (2011).
55. GB 5085.3-2007, Identification Standard for Hazardous Wastes - Identification for Extraction Toxicity (2007).
56. H. Y. Hu, H. Liu, W. Q. Shen, G. Q. Luo, A. J. Li, Z. L. Lu and H. Yao, *Chemosphere*, **93**, 590 (2013).
57. T. W. Cheng and Y. S. Chen, *Chemosphere*, **51**, 817 (2003).
58. Y. Yang, Y. Xiao, N. Wilson and J. H. L. Voncken, *J. Hazard. Mater.*, **166**, 567 (2009).
59. Z. Aksu and I. A. Isoglu, *Process Biochem.*, **40**, 3031 (2005).
60. A. M. Zayed, A. Q. Selim, E. A. Mohamed, M. S. M. A. Wahed, M. K. Seliem and M. Sillanpaa, *Appl. Clay Sci.*, **140**, 17 (2017).
61. Z. C. Ma and Y. B. Xie, *Chem. Res. Appl.* (In Chinese), **13**, 417 (2001).
62. https://www.dowater.com/Tech/2019-10-21/1082324.html, (In Chinese) (Accessed October 27th 2020).

Supporting Information

Adsorption performance and mechanism investigation of Mn^{2+} by facile synthesized ceramsites from lime mud and coal fly ash

Changjin Ou, Suwan Dai, Shuxuan Li, Jie Xu, and Juan Qin†

Nantong Key Laboratory of Intelligent and New Energy Materials, School of Chemistry and Chemical Engineering, Nantong University, Nantong 222100, China

(*Received 29 June 2020 • Revised 28 October 2020 • Accepted 3 November 2020*)

Table S1. The nomenclature and composition of the investigated samples (wt%)

Sample No.	Lime mud	Coal fly ash
L50	50	50
L60	60	40

Table S2. Physical properties of the investigated ceramsites

Sample No.	Bulk density (g/cm^3)	Water adsorption (%)	Apparent porosity (%)	Cylinder compressive strength (MPa)
L50	0.88±0.11	30.15±0.79	48.57±1.32	10.59±1.86
L60	0.72±0.08	44.44±1.13	52.02±1.43	8.98±0.97

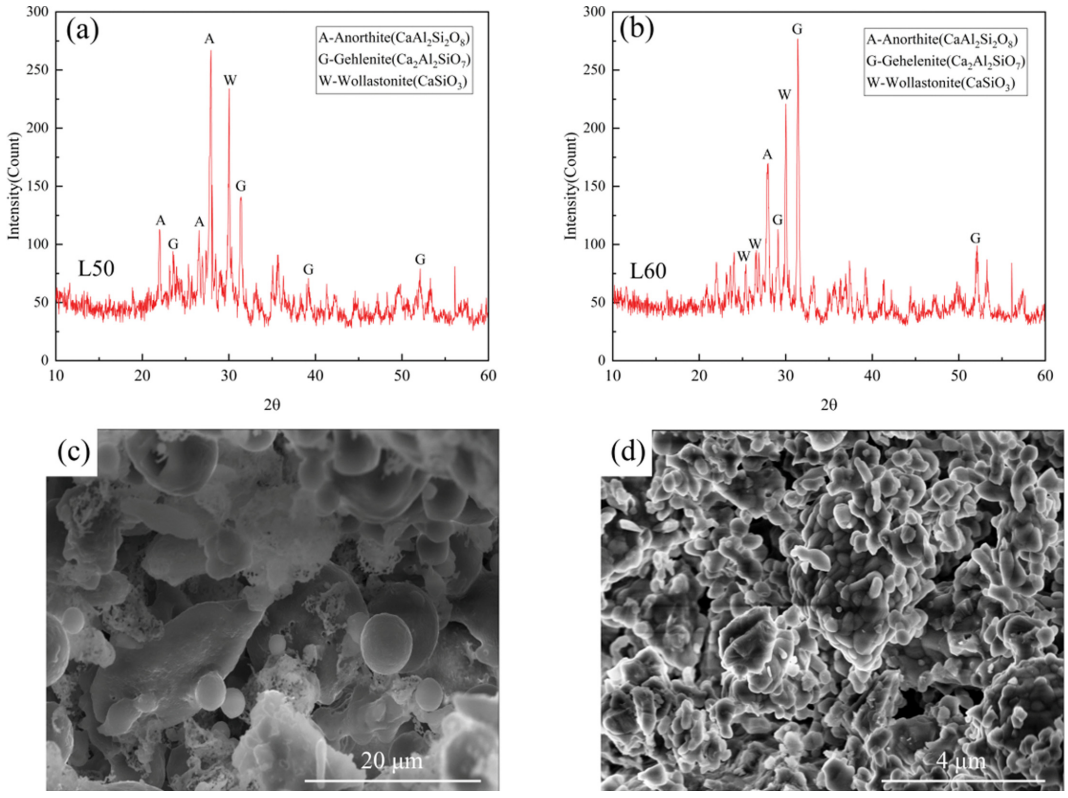

Fig. S1. XRD patterns and SEM images of ceramsites: (a) XRD of L50; (b) XRD of L60; (c) SEM of L50; (d) SEM of L60.